Capturing the Pattern of Transition From Carrier to Affected in Leber Hereditary Optic Neuropathy

MICHELE CARBONELLI, CHIARA LA MORGIA, MARTINA ROMAGNOLI, GIULIA AMORE, PIETRO D'AGATI, MARIA LUCIA VALENTINO, LEONARDO CAPORALI, MARIA LUCIA CASCAVILLA, MARCO BATTISTA, ENRICO BORRELLI, ANTONIO DI RENZO, VINCENZO PARISI, NICOLE BALDUCCI, VALERIO CARELLI, AND PIERO BARBONI

• PURPOSE: To capture the key features patterning the transition from unaffected mutation carriers to clinically affected Leber hereditary optic neuropathy (LHON), as investigated by optical coherence tomography.
• DESIGN: Observational case series.
• METHODS: Four unaffected eyes of 4 patients with LHON with the first eye affected were followed across conversion to affected, from 60 days before to 170 days after conversion. The primary outcome measures were multiple timepoints measurements of peripapillary retinal nerve fiber layer (RNFL) thickness for temporal emiside of the optic nerve (6 sectors from 6-11, clockwise for the right eye and counterclockwise for the left eye) in all patients and nasal emi-macular RNFL and ganglion cell layer (GCL) thickness in 2 patients.
• RESULTS: While the presymptomatic stage was characterized by a dynamic thickening of sector 8, the beginning of the conversion coincided with an increase in the thickness of the sectors bordering the papillo-acular bundle (6 and 7 for the inferior sectors, 10 and 11 for the superior sectors) synchronous with the thinning of sectors 8 and then 9. Conversely, the GCL did not undergo significant changes until the onset of visual loss when a significant reduction of thickness became evident.
• CONCLUSION: In this study we demonstrated that the thinning of sector 8 can be considered the structural hallmark of the conversion from the presymptomatic to the affected state in LHON. It is preceded by its own progressive thickening extending from the optic nerve head toward the macula and occurs regardless of the amount of swelling of the rest of the peripapillary fibers. (Am J Ophthalmol 2022;241: 71–79. © 2022 The Authors. Published by Elsevier Inc. This is an open access article under the CC BY-NC-ND license (http://creativecommons.org/licenses/by-nc-nd/4.0/))

LEBER HEREDITARY OPTIC NEUROPATHY (LHON) IS THE most common inherited mitochondrial disorder and usually affects young males.[1] It is characterized by selective neurodegeneration of retinal ganglion cells (RGCs) and their axons, which typically leads to bilateral centrocecal scotoma due to preferential loss of papillomacular bundle nerve fibers.[2] The primary mechanism of neurodegeneration is centered on the mitochondrial dysfunction induced by 1 of 3 frequent maternally inherited mitochondrial DNA point mutations affecting complex I subunit genes.[3]

As LHON is characterized by incomplete penetrance, the disease clinically presents an asymptomatic stage, which may last through a lifetime in more than half of the mutation carriers. These asymptomatic individuals may present, however, with typical funduscopic changes including swelling of the peripapillary retinal nerve fiber layer (pRNFL) and microangiopathy.[4,5] Both may be related and part of a compensatory effect that may involve mitochondrial biogenesis.[6]

The conversion from the asymptomatic to the symptomatic stage begins typically as a unilateral subacute optic neuropathy with, in most cases, subsequent asynchronous involvement of the second eye.[7] The nature of the disease natural history makes it challenging and uncommon to detect the early structural and functional changes related to the disease conversion, which remains substantially uncharacterized in its granular details.

Only a few longitudinal spectral-domain optical coherence tomography (SD-OCT) studies have described the natural history of pRNFL and ganglion cell layer (GCL) changes during conversion of LHON, highlighting 2 important observations: 1) thickening and subsequent thinning of the pRNFL, which starts in the temporal and infe-

AJO.com Supplemental Material available at AJO.com.
Accepted for publication April 22, 2022.

From the Neurology Unit (M.C., G.A., M.L.V., V.C.), Department of Biomedical and Neuromotor Sciences, University of Bologna, Bologna; IRCCS Istituto delle Scienze Neurologiche di Bologna (C.L.M., M.R., P.D., M.L.V., L.C., V.C.), Programma di Neurogenetica, Bologna; Department of Ophthalmology (M.L.C., M.B., E.B., P.B.), University Vita-Salute, IRCCS San Raffaele Scientific Institute, Milan; IRCCS Fondazione Bietti (A.D.R., V.P.), Rome; Studio Oculistico d'Azeglio (N.B., P.B.), Bologna, Italy

Inquiries to Michele Carbonelli, Department of Biomedical and Neuromotor Sciences, University of Bologna, Via Altura 3, 40139 Bologna, Italy; or Piero Barboni, Department of Ophthalmology, University Vita-Salute, IRCCS Ospedale San Raffaele, Via Olgettina, 60 Milan, Italy.; e-mail: dmcarbonelli@gmail.com, p.barboni@studiodazeglio.it

0002-9394/$36.00
https://doi.org/10.1016/j.ajo.2022.04.016

rior quadrants and propagates to the other quadrants,[8] and 2) early nasal GCL thinning with the progressive involvement of other sectors fitting the distribution of papillomacular fibers.[9]

Other cross-sectional studies analyzed the progressive thinning of RNFL and GCL in acute and chronic stages and confirmed the typical pattern of RNFL loss caused by the disease and the preferential involvement of papillomacular bundle fibers.[10,11,12] However, there is a dearth of studies addressing the relationship between RGC degeneration and fiber swelling, which would inform on their reciprocal role during the early phases of developing loss of vision. The new swept-source OCT device has greater temporal and spatial interpolation of data and allows us to obtain a better structural and topographical analysis of retinal layers.

In this study, we analyzed 4 eyes from 4 patients in the presymptomatic stage after involvement of the first eye. Our aim was to describe the transition from presymptomatic to subacute changes of RNFL and GCL, highlighting their temporal and topographic relationship in the attempt to gain further pathophysiologic insights about the key events occurring during disease conversion.

METHODS

All patients included in the present study (3 males and 1 female) had a molecularly confirmed diagnosis of LHON (3 patients had the m.11778G>A/*MT-ND4* mutation and 1 patient had m.3460G>A/*MT-ND1*) and belonged to 4 unrelated pedigrees.

We recruited the patients when the first eye was already involved and the second still asymptomatic, and we included in the analysis the fellow asymptomatic eye of each patient across presymptomatic to subacute stages with long follow-up times. We defined the onset of the visual symptoms as the subjectively reported visual impairment before the first objectively documented decrease of visual acuity (above logarithm of the minimum angle of resolution 0) accompanied by a corresponding visual field defect in central vision. The patients underwent an extensive ophthalmologic examination, including best corrected visual acuity (VA) measurement, slit-lamp examination, intraocular pressure measurement, indirect ophthalmoscopy, and optic nerve head photography, automated visual field test (VF) (Humphrey Field Analyzer; Zeiss, San Leandro, CA). Eyes with the presence of any retinal pathology and/or optic nerve disease other than LHON, spherical and/or cylindrical refractive errors >3 and 2 diopters, respectively, and systemic conditions that may affect the vascular system were excluded. Patients gave their informed consent according to the Declaration of Helsinki, and the local Ethical Committee at the IRCCS Istituto delle Scienze Neurologiche di Bologna approved the study (121-2019 OSS AUSL BO).

• **INSTRUMENTATION AND PROCEDURES:** OCT images were taken using 2 different devices: SS-OCT (DRI-OCT; Triton, Tokyo, Japan) and SD-OCT (Cirrus HD-OCT; Carl Zeiss Meditec, Inc, Dublin, CA).

The SS-OCT uses a wavelength of 1050 nm with a scan speed of 100,000 A-scans per second. The images were obtained using a 3-dimensional wide scan protocol with a size of 12 mm × 9 mm consisting of 256 B-scans, each comprising 512 A-scans. This allowed obtaining images of the macular and optic nerve head region in a single scan. The total acquisition time was 1.3 s per 12 mm × 9 mm scan. Following proper seating and alignment of each patient, the iris was brought into view using the mouse-driven alignment system, and the ophthalmoscopic image was focused. The analysis algorithm processed data from 3-dimensional volume scans with measured thicknesses of the macular and peripapillary regions. OCT protocols included the evaluation of the pRNFL, macular RNFL, and macular GCL. pRNFL thickness was measured with a 360° 3.46-mm–diameter circle scan centered automatically around the optic disc and across 8 sectors according to Early Treatment Diabetic Retinopathy Study (ETDRS) centered on the fovea in macular region.[13] The segmentation analysis of the macula measured across 6 sectors (superotemporal, superior, superonasal, inferonasal, inferior, and inferotemporal) of the 6-mm–diameter circular annulus centered on the fovea included the GCL between the macular RNFL and the inner nuclear layer boundaries. The built-in SS-OCT eye-tracking system was used to provide reproducible measurements.

SD-OCT uses a wavelength of 840 nm with a scan speed of 27,000 A-scans per second. All scans were acquired using the Optic Disc Cube 200 × 200 protocol. To acquire the Optic Disc Cube, the ONH was centered on the live image and centering and enhancement were optimized. After the scanning process was launched, the instrument's laser beam generated a cube of data measuring 6 mm × 6 mm after scanning a series of 200 B-scans with 200 A-scans per B-scan (40,000 points) in 1.5 seconds (27,000 A-scans/s). Cirrus SD-OCT algorithms were used to find the optic disc and automatically place a calculation circle of 3.46-mm diameter symmetrically around it. The system extracted from the data cube 256 A-scan samples along the path of the calculation circle.

All images were acquired by an experienced operator (M.C.) with both devices. The quality of each scan and accuracy of the segmentation algorithm were reviewed by experienced and blinded examiners (P.B., V.P., C.L.M., N.B.). Images with segmentation failures, significant motion artefacts, or signal strength <6 were excluded.

The pRNFL scan circle was segmented into 12 sectors clockwise for the right eye and counterclockwise for the left eye, to preserve the same topographic correspondence in each eye examined. We included, for the analysis, multiple time point measurements of pRNFL thickness for temporal emi-side of the optic nerve (6 sectors from 6-11) in all

patients and nasal emi-macular pRNFL (nasal and inferior) and GCL (superonasal, inferonasal, and inferior) thickness for 2 patients.

• **STATISTICAL ANALYSIS:** Due to the nature of the study, patients are described individually, without calculating inferential statistics.

The trend over time of the thickness with respect to the baseline (first examination) is shown for each patient (Figures 1A, through Figure 4A).

Furthermore, we evaluated the percentage variations of the thicknesses with respect to the baseline for each patient, and then these were plotted (Figure 1B, through Figure 4B and Figures 5 and 6).

RESULTS

• **DEMOGRAPHIC DATA:** Table 1 shows the demographic data and clinical features of the 4 patients with LHON. We studied these 4 patients across the conversion of the unaffected eye (second eye). After the disease conversion (onset), the examinations were uniformly performed at 10 days, 1 month, about 2 months, and at least a final visit at about 6 months. We had available also different time points preceding the onset, which provided information on the preclinical stage immediately before conversion (Supplemental Figure S1). In patients undergoing SS-OCT (patients 1 and 2), both RNFL (peripapillary and macular) and GCL were examined while in patients undergoing HD-OCT only pRNFL was examined.

Before the baseline examination each patient was already undergoing LHON therapy, which was started after the LHON diagnosis: 3 patients were treated with idebenone[14] and 1 patient with the antioxidant alfa-tocotrienol vatiquinone.[15]

• **CLOCK-HOUR SECTORS OF TEMPORAL PRNFL ANALYSIS:**

Patient 1

Before the onset of visual symptoms, we detected a gradual pRNFL thickening starting first with sectors 7 and 8 (−40 days) followed by a progressive thickening of sector 6 (−20 days) (Figure 1). At the onset of clinical symptoms, subjectively perceived as visual impairment, notably there was a rapid thickening of the sectors 9 and 10. This event, in conjunction with the progression of thickening in sectors 6 and 7, coincided with the thinning of sector 8, the first to invert the progression, followed later by sector 9, the second to display the same fate (within the first month). By the second month, pRNFL thickness was consistently reduced across all sectors except sector 11, with a hierarchy of the topographic pattern characterized by sectors 7 and 10, adjacent to the papillomacular bundle, going first, followed by the most external ones (sectors 6 and 11).

Thus, the first sectors reaching back the thickness at baseline were sectors 8 and 9, followed by 7 and 10, and finally 6 and 11.

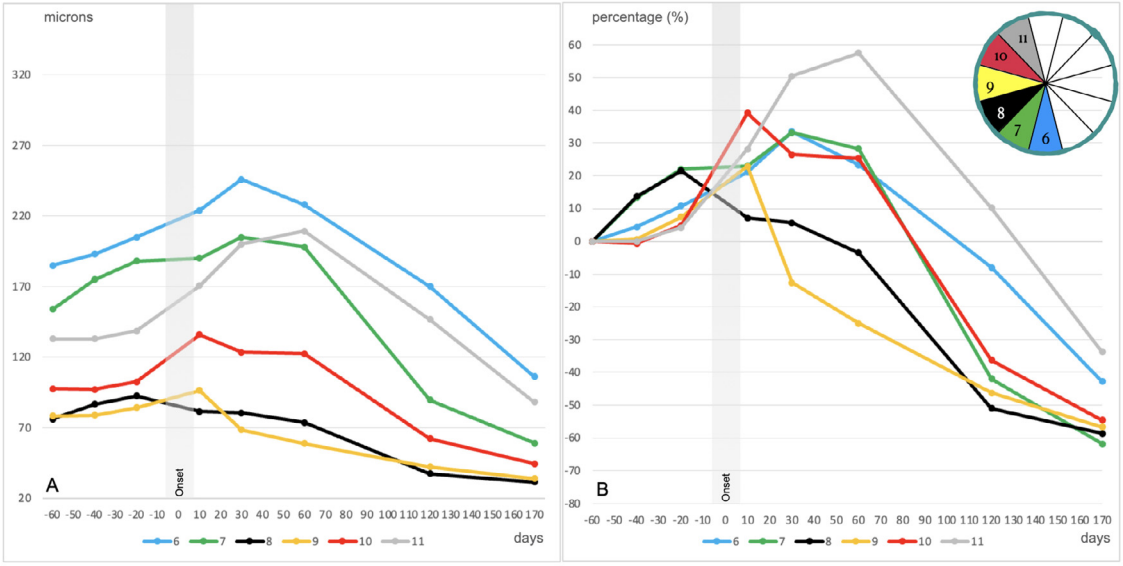

FIGURE 1. Longitudinal analysis of temporal peripapillary retinal nerve fiber layer of patient 1. (A) Thickness change and (B) percentage change in thickness from baseline (first examination).

TABLE 1. Demographic Data and Clinical Features of the 4 Patients With Leber Hereditary Optic Neuropathy

	Patient 1	Patient 2	Patient 3	Patient 4
Age at onset (y)	15	22	19	16
Gender	Male	Male	Female	Male
Mutation	11778/ND4	11778/ND4	3460/ND1	11778/ND4
Interval between eyes' onset (days)	140 days	151 days	229 days	10 days
Therapy before second eye' onset (days) (dose)	42 (idebenone 900 mg/day)	80 (idebenone 900 mg/day)	60 (vatiquinone 900 mg/day)	10 (idebenone 900 mg/day)
Visual acuity at final visit (logMAR)	1.8	1.32	1.3	1.3

logMAR = logarithm of the minimum angle of resolution.

Patient 2

Patient 2 displayed an increase in fiber thickness before symptoms (−10 days), which was initially noticeable and fast only in sectors 6 and 9. At onset, a further thickening of the external sectors 6, 7, 10, and 11 was concomitant to thinning of sectors 8 and 9. Therefore, the first sector to undergo atrophy was sector 8, coinciding with the onset of symptoms, followed by sector 9, whereas sector 7 remained essentially stable. At month 1, only sector 11 continued to thicken, and at month 2 all sectors reverted toward a decrease in thickness, following the same topographic pattern as in patient 1 (Figure 2).

Patient 3

Before the onset of symptoms, we detected a gradual pRNFL thickening, marked and rapid in the external sectors (6, 7, 10, and 11) and barely noticeable in the papillomacular bundle sectors (8 and 9). Shortly before clinical onset, a rapid thickening of sector 6 followed by sector 10 preceded the thinning of sectors 8 and 9. Therefore, the first sector to progress toward atrophy was sector 8 coincidentally with the onset of symptoms, followed by sector 9 soon after onset (+20 days). Furthermore, sector 7 remained essentially stable across the onset. By the second month, pRNFL thickness began to reduce in all sectors, except sector 11, first those adjacent to the papillomacular bundle (sectors 7 and 10) and then the more external ones (sectors 6 and 11).

The first reaching the baseline thickness were sectors 8 and 9, followed by 7 and 10, and finally 6 and 11, consistent with the pattern already described in patients 1 and 2 (Figure 3).

Patient 4

Since the baseline assessment for this patient was close to the clinical onset, at the first follow-up (+10 days) the thinning of sectors 8 and 9 was noticeable and the thickening of the remaining sectors was more marked in the external ones (7, 10, 6, and 11).

Thus, the first sector to progress toward atrophy was sector 8 in coincidence with the onset of symptoms, followed by sector 9. Sector 7 remained essentially stable until month 2, when it started to undergo toward atrophy and at month 4 only the most external sectors were still above the baseline value (sectors 6 and 11) (Figure 4). This pattern is again consistent to what we observed for the other 3 patients.

Common features in all patients

Overall, in all patients, the beginning of the conversion coincided with an abrupt reversal of the pRNFL swelling. What we observed at this turning point was an increase in the thickness of the sectors bordering the papillomacular bundle (6 and 7 for the inferior sectors, 10 and 11 for the superior) synchronous with the thinning of sectors 8 and then 9. This is further highlighted by harmonizing the 3 patients having the same time point available at −20 days (Supplemental Figure S2). This is the structural

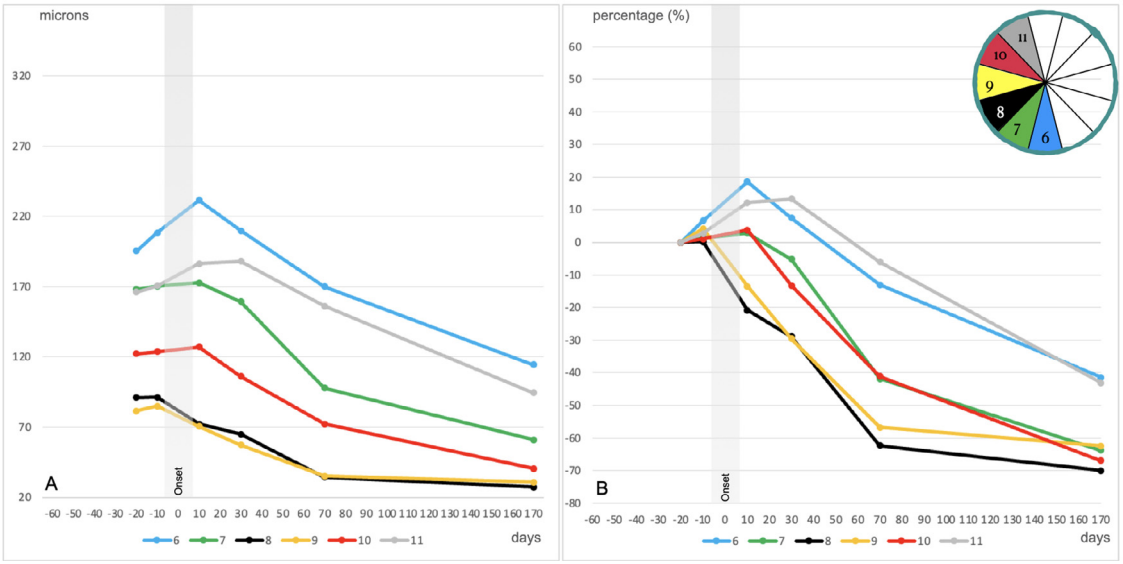

FIGURE 2. Longitudinal analysis of temporal peripapillary retinal nerve fiber layer of patient 2. (A) Thickness change and (B) percentage change in thickness from baseline (first examination).

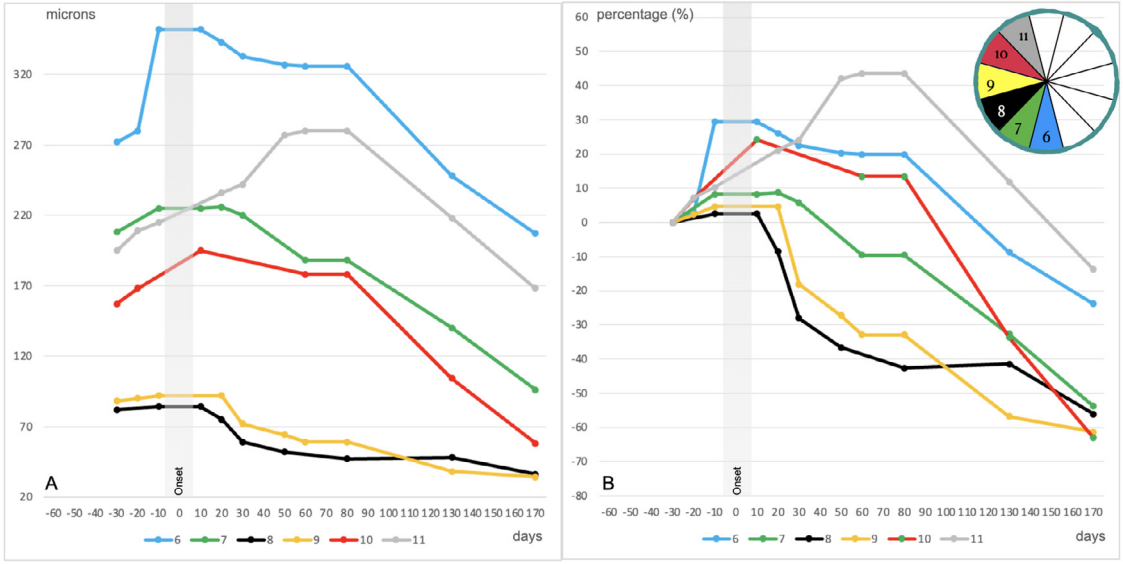

FIGURE 3. Longitudinal analysis of temporal peripapillary retinal nerve fiber layer of patient 3. (A) Thickness change and (B) percentage change in thickness from baseline (first examination).

OCT sign that invariably indicated the irreversible onset of the visual symptoms in all patients, the key transition in the conversion from preclinical to symptomatic. This is reflected by the common pattern of how pRNFL thickness returns to baseline, consistent in all patients by the sequence of sectors 8, 9, followed by 7 and 10, and finally 6 and 11.

• **MACULAR RNFL ANALYSIS ACCORDING TO ETDRS:** In the 2 patients investigated by SS-OCT (patients 1 and 2), the analysis of inferior and nasal macular RNFL quadrants (topographic site of the papillomacular bundle) divided according to ETDRS into 2 concentric rings revealed an earlier thickening of the outer ring than the inner one (Figure 5).

• **GANGLION CELL LAYER ANALYSIS:**

Common features

The GCL did not undergo significant changes until the onset of visual loss when a significant reduction of thickness

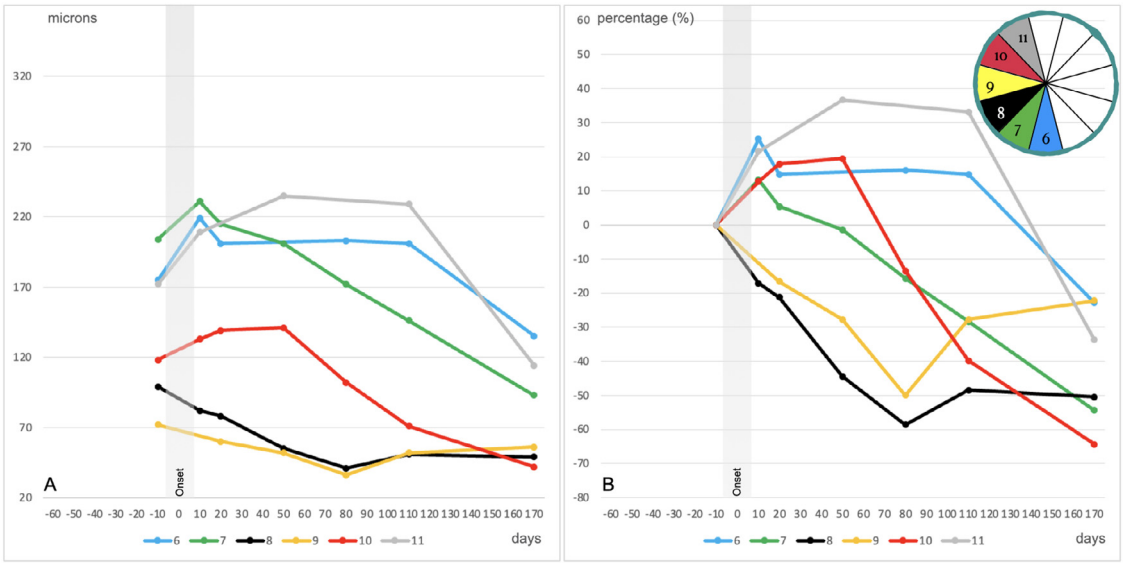

FIGURE 4. Longitudinal analysis of temporal peripapillary retinal nerve fiber layer of patient 4. (A) Thickness change and (B) percentage change in thickness from baseline (first examination).

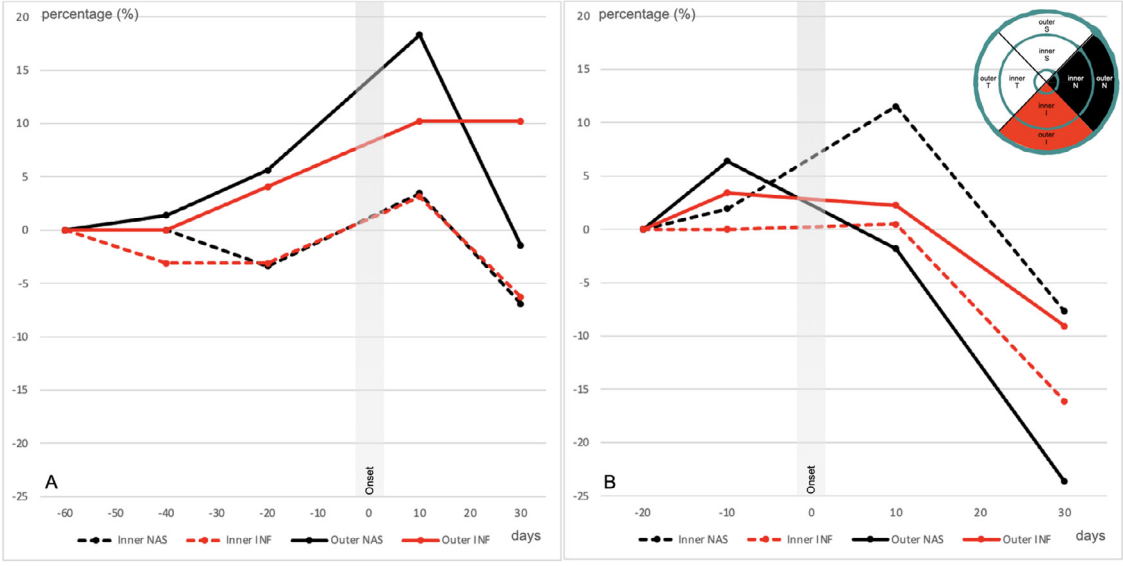

FIGURE 5. Percentage change of the macular retinal nerve fiber layer thickness from baseline (first examination) of patients 1 (A) and patient 2 (B). The analysis of inferior and nasal macular retinal nerve fiber layer quadrants is divided according to Early Treatment Diabetic Retinopathy Study in the inner and outer concentric rings. INF = inferior NAS = nasal.

became evident. The nasal sectors underwent the greatest and fastest atrophy in the first month after onset, losing about 20% of thickness from baseline and progressively each sector reached atrophy with reduction of thickness ranging between −30% and −40% from baseline at the end of follow-up (Figure 6).

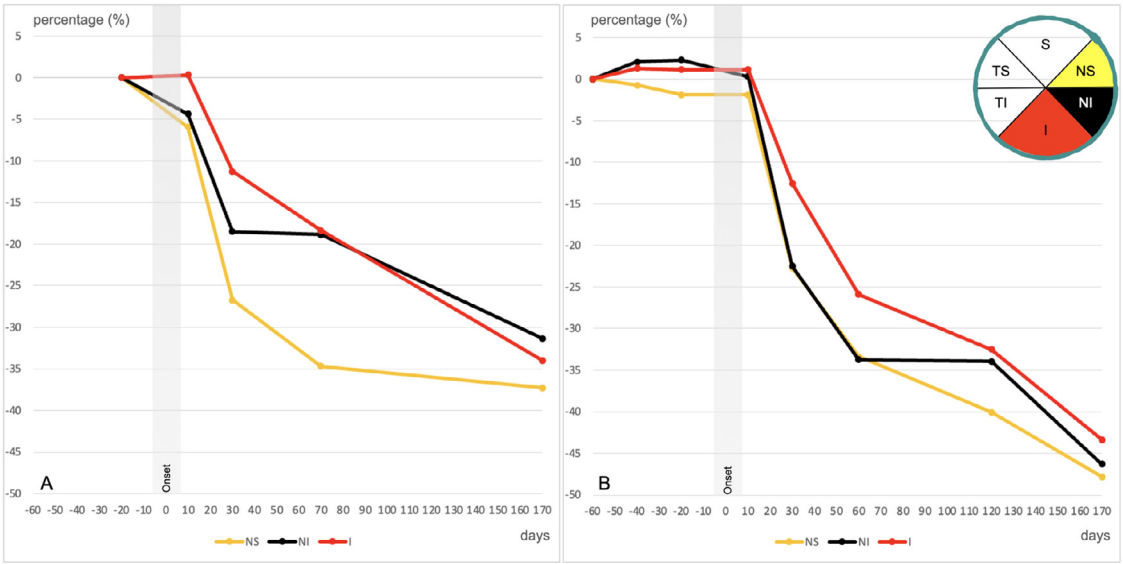

FIGURE 6. Percentage change of ganglion cell layer thickness of nasal and inferior sectors from baseline (first examination) of patient 1 (A) and patient 2 (B). I = inferior; NI = inferonasal; NS = superonasal; S = superior; TI = inferotemporal; TS = superotemporal.

DISCUSSION

In this study we described a consistent structural event marking the conversion from presymptomatic to affected status in LHON. This hallmark consists in the RNFL thinning of the temporal sectors (sector 8 first and then 9), which invariably occurs when the contiguous sectors 6 and 7 and 10 and 11 increase their thickness. This seems to occur independently from the amount of fiber swelling, which varies from patient to patient. In the patient with the longest presymptomatic follow-up (−60 days), it is also remarkable that sector 8 presents with an early dynamic progression of thickening, which only then spreads to the contiguous sectors 6 and 7 and 10 and 11, leading to the sudden thinning of sector 8, marking the onset of visual loss. Finally, the ETDRS ring macular RNFL analysis supported that RNFL swelling spreads from the optic nerve head toward the macula, suggesting that the structural changes are evident first in the axons, subsequently affecting the RGC cell body. Differently, at the same stage, the GCL did not show any significant changes in thickness. Overall, our observations provide the understanding of events that should be considered red flags of conversion in asymptomatic carriers, potentially defining a further window of opportunity for early therapeutic interventions aimed to abort the disease onset by stopping this mechanism.

Our observations also raise the question of what mechanism dictates the conversion. The swelling of fibers begins in the inferior sectors of the papillomacular bundle and extends to the periphery, propagating to the fibers at the poles and then to the nasal ones, raising the possibility that this event may cause a compression phenomenon on the most vulnerable thinner axons of sectors 8 and then 9. The sectors that first adapted to the energy deficit by compensatory mechanism that could underlie swelling, are then the first to be damaged in a "boomerang" type mechanism.

Interestingly, in all patients, the average thickness of sector 7 remained stable during onset, probably because the fibers closest to sector 8 are decreasing and those closest to sector 6 are increasing.

When examining the pRNFL subdivided into quadrants only, the thinning of the lower part of the temporal quadrant (sector 8) can be compensated for by the swelling of the rest of the temporal quadrant, thus keeping the average thickness constant and masking the damage already occurring, unraveled only by the sector analysis. Consequently, the study of the clock hour sectors is crucial as the conversion phase is ophthalmoscopically masked by hyperemia and microangiopathy of the optic disc, hiding the presence of any objective sign of RNFL atrophy. Therefore, identifying this event marking visual decline allows us to accurately date the onset of symptoms, which frequently arise insidiously and therefore subjectively misunderstood by the patient. We may suggest that, during the follow-up of asymptomatic carriers, any changes other than sector 8 thinning might be reversible, but once sector 8 underwent atrophy this irreversibly leads to the onset of visual symptoms.

Remarkably, despite the 4 patients having different mitochondrial DNA mutations, different degrees of RNFL swelling in terms of quantity and duration, and different du-

ration and type of treatment, they consistently followed the same pattern with similar key characteristics.

However, the GCL did not show any significant changes in thickness in the phase preceding clinical onset when the GCL atrophy starts first in the nasal sector. In fact, the swelling of fibers in the presymptomatic phase, greater and more persistent in some patients (such as patient 1), influenced the subsequent atrophic phase of the RNFL, which occurred later without however affecting the dynamics of GCL changes.

Furthermore, the amount of thickening does not affect the clinical course of the disease, which consistently followed similar steps in all patients with LHON with vision loss reaching nadir between 3 and 6 months (Table 1).[2]

Analyzing the macular RNFL according to the ETDRS, there is some indication that the fibers of the outer ring might be the first to be affected by the swelling. This, therefore, suggests that the first detectable axonal change needs to be searched in the papillary/peripapillary region and not in the macula.

Overall, this study connects for the first time the assessment of pRNFL and GCL, confirming our earlier study describing the natural history of pRNFL changes,[8] adding much greater detail in the conversion events. At the same time, the current study partially corrects our previous observations claiming that the very first event in conversion is RGC loss in the macular region.[9] The temporal relationship between axonal swelling retrogradely propagating from the optic disc to the macula is consistent with the previously hypothesized impairment of axonal transport in conjunction with the compensatory increase of mitochondrial biogenesis.[6] This possibly engulfs the axons, contributing to their swelling and ultimately signaling the catastrophic events leading to RGC apoptotic death.[2] Alternatively, but not mutually exclusive, there is also the possibility of a compartment effect within the retrolaminar optic nerve, which reflects retrogradely in the axons entering the optic disc, thus contributing to the swelling progression. No matter which mechanism generates the axonal swelling, the most evident structural changes that can be followed by OCT, it remains to be understood and clarified the triggering event that determines the switch from asymptomatic to clinically affected that we here documented at the structural level.

This study has 2 limitations, ie, we analyzed only 4 patients and we used 2 different OCT machines and technologies. This is quite unavoidable when we are to catch such a narrow temporal window of opportunity in the natural history of LHON. However, we remain reassured by the consistency of our observations across patients and OCT machines.

In conclusion, our detailed analysis by sectors of the events occurring over time at the peripapillary RNFL and at the macula allowed the detection of the timing and localization of structural changes marking the transition from the asymptomatic to the symptomatic stages of LHON. This not only provides a marker for the conversion but also a window for the earliest possible treatment. As our patients were all treated with antioxidants that did not abort the disease in the second eye, other pathogenetic mechanisms other than reactive oxygen species need to be targeted for the therapy to be successful.

ALL AUTHORS HAVE COMPLETED AND SUBMITTED THE ICMJE FORM FOR DISCLOSURE OF POTENTIAL CONFLICTS OF INTEREST.
Funding/Support: This work was supported by the Italian Ministry of Health (grant GR-2016-02361449 to L.C. and "Ricerca Corrente" funding to V.C. and V.P.).
Financial Disclosures: M.C. has been a consultant for GenSight Biologics and Santhera Pharmaceuticals; received speaker honoraria from First Class srl, and is subinvestigator for clinical trials sponsored by GenSight Biologics and by Santhera Pharmaceuticals. None of these activities are related to conducting this study and writing the manuscript. C.L.M. has been a consultant for Chiesi Farmaceutici, Regulatory Pharma Net, and Thenewway srl; received speaker honoraria from Santhera Pharmaceuticals, Chiesi Farmaceutici, Regulatory Pharma Net, Thenewway srl, First Class srl, and Biologix; and is principal investigator/subinvestigator for clinical trials sponsored by GenSight Biologics and by Santhera Pharmaceuticals. None of these activities are related to conducting this study and writing the manuscript. M.R. has been a consultant for GenSight Biologics, received speaker honoraria from Santhera Pharmaceuticals, and is study coordinator for clinical trials sponsored by GenSight Biologics and Santhera Pharmaceuticals. None of these activities are related to conducting this study and writing the manuscript. G.A. is a subinvestigator for clinical trials sponsored by GenSight Biologics and Santhera Pharmaceuticals. None of these activities are related to conducting this study and writing the manuscript. L.C. received speaker honoraria from First Class srl and University of Parma. None of these activities are related to conducting this study and writing the manuscript. M.L.C. received speaker honoraria from Chiesi Farmaceutici. None of these activities are related to conducting this study and writing the manuscript. V.P. received speaker honoraria from Omikron Italia. None of these activities are related to conducting this study and writing of the manuscript. V.C. reports consultancies and advisory board activities with GenSight Biologics, Pretzel Therapeutics, Stealth Biotherapeutics, and Chiesi Farmaceutici; speaker honoraria from Chiesi Farmaceutici, First Class srl, and Medscape; and is principal investigator/subinvestigator for clinical trials sponsored by GenSight Biologics and by Santhera Pharmaceuticals. None of these activities are related to conduction of this study and the writing of the manuscript. P.B. reports consultancies for GenSight Biologics and received speaker honoraria from Santhera Pharmaceuticals, Chiesi Farmaceutici, and Omikron Italia and is a subinvestigator for clinical trials sponsored by GenSight Biologics and Santhera Pharmaceuticals. None of these activities are related to conduction of this study and the writing of the manuscript. All other authors indicate no financial support or conflicts of interest. All authors attest that they meet the current ICMJE criteria for authorship.
Acknowledgments: We are deeply indebted with all our patients, who offered the maximal collaboration and support to our research project. We thank MITOCON and the representative of LHON patient community in Italy, Paula Morandi.

REFERENCES

1. Newman N. Hereditary optic neuropathies. In: Miller NR, Biousse V, Newman NJ, Kerrison JB, eds. Walsh and Hoyt's Clinical Neuro-Ophthalmology. Philadelphia: Lippincott Williams & Wilkins; 2005:465–501.
2. Carelli V, Ross-Cisneros FN, Sadun AA. Mitochondrial dysfunction as a cause of optic neuropathies. *Prog Retin Eye Res*. 2004;23:53–89.
3. Maresca A, Caporali L, Strobbe D, et al. Genetic basis of mitochondrial optic neuropathies. *Curr Mol Med*. 2014;14:985–992.
4. Nikoskelainen E, Hoyt WF, Nummelin K. Ophthalmoscopic findings in Leber's hereditary optic neuropathy. I. Fundus findings in asymptomatic family members. *Arch Ophthalmol*. 1982;100:1597–1602.
5. Nikoskelainen E, Hoyt WF, Nummelin K. Ophthalmoscopic findings in Leber's hereditary optic neuropathy: II. The fundus findings in the affected family members. *Arch Ophthalmol*. 1983;101:1059–1068.
6. Giordano C, Iommarini L, Giordano L, et al. Efficient mitochondrial biogenesis drives incomplete penetrance in Leber's hereditary optic neuropathy. *Brain*. 2014;137(2):335–353.
7. Riordan-Eva P, Sanders MD, Govan GG, et al. The clinical features of Leber's hereditary optic neuropathy defined by the presence of a pathogenic mitochondrial DNA mutation. *Brain*. 1995;118:319–337.
8. Barboni P, Carbonelli M, Savini G, et al. Natural history of Leber's hereditary optic neuropathy: longitudinal analysis of the retinal nerve fiber layer by optical coherence tomography. *Ophthalmology*. 2010;117:623–627.
9. Balducci N, Savini G, Cascavilla ML, et al. Macular nerve fiber and ganglion cell layer changes in acute Leber's hereditary optic neuropathy. *Br J Ophthalmol*. 2016;100:1232–1237.
10. Monster SJ, Moster ML, Bryan MS, et al. Retinal ganglion cell and inner plexiform layer loss correlate with visual acuity loss in LHON: a longitudinal, segmentation OCT analysis. *IOVS*. 2016;57(8):3872–3883.
11. Hwang TJ, Karanjia R, Moraes-Filho MN, et al. Natural history of conversion of Leber's hereditary optic neuropathy: a prospective case series. *Ophthalmology*. 2017;124(6):843–850.
12. Wang D, Liu HL, Du YY, et al. Characterisation of thickness changes in the peripapillary retinal nerve fibre layer in patients with Leber's hereditary optic neuropathy. *Br J Ophthalmol*. 2021;105(8):1166–1171. doi:10.1136/bjophthalmol-2020-316573.
13. Early Treatment Diabetic Retinopathy Study Research GroupGrading diabetic retinopathy from stereoscopic color fundus photographs—an extension of the Modified Airlie House Classification: ETDRS report number 10. *Ophthalmology*. 1991;98:786–806.
14. Klopstock T, Yu-Wai-Man P, Dimitriadis K, et al. A randomized placebo-controlled trial of idebenone in Leber's hereditary optic neuropathy. *Brain*. 2011;134(pt 9):2677–2686.
15. Sadun AA, Chicani CF, Ross-Cisneros FN, et al. Effect of EPI-743 on the clinical course of the mitochondrial disease Leber hereditary optic neuropathy. *Arch Neurol*. 2012;69(3):331–338. doi:10.1001/archneurol.2011.2972.